Nonlinear post-fire simulation of concentrically loaded rectangular thin-walled concrete-filled steel tubular short columns accounting for progressive local buckling

Kamil, G. M., Liang, Q. Q. and Hadi, M. N. S. (2019). Nonlinear post-fire simulation of concentrically loaded rectangular thin-walled concrete-filled steel tubular short columns accounting for progressive local buckling. *Thin-Walled Structures*, 145: 106423.

Nonlinear post-fire simulation of concentrically loaded rectangular thin-walled concrete-filled steel tubular short columns accounting for progressive local buckling

Ghanim Mohammed Kamil[a], Qing Quan Liang[a,*], Muhammad N. S. Hadi[b]

[a] *College of Engineering and Science, Victoria University, PO Box 14428, Melbourne, VIC 8001, Australia*

[b] *School of Civil, Mining and Environmental Engineering, University of Wollongong, Wollongong, NSW 2522, Australia*

Abstract

The repair of fire-damaged thin-walled rectangular concrete-filled steel tubular (CFST) columns in engineering structures after fire exposure requires the assessment of their residual strength and stiffness. Existing numerical models have not accounted for the effects of local buckling on the post-fire behavior of CFST columns with rectangular thin-walled sections. This paper describes a nonlinear post-fire simulation technique underlying the theory of fiber analysis for determining the residual strengths and post-fire responses of concentrically loaded short thin-walled rectangular CFST columns accounting for progressive local buckling. The post-fire stress-strain laws for concrete in rectangular CFST columns are proposed based on available test data and implemented in the theoretical model. An innovative numerical scheme for modeling the progressive local and post-local buckling of CFST thin-walled columns is discussed. The nonlinear post-fire simulation model is verified by experimental data and then used to investigate the significance of local buckling, material strengths and width-to-thickness ratio on the post-fire responses of CFST stub columns. The proposed post-fire computer model

* Corresponding author.
E-mail address: Qing.Liang@vu.edu.au (Q. Q. Liang)

is shown to be capable of predicting well the residual stiffness and strength of concentrically loaded thin-walled CFST columns after fire exposure. A design formula is proposed that estimates well the post-fire residual strengths of CFST columns. Computational results presented provide a better understanding of the post-fire behavior of CFST columns fabricated by thin-walled sections incorporating local and post-local buckling.

Keywords: Concrete-filled steel tubes; Local and post-local buckling; Nonlinear post-fire analysis; Residual strength.

1. Introduction

Rectangular concrete-filled steel tubular (CFST) columns fabricated with thin-walled sections as shown in Fig. 1 are widely used in tall buildings to support heavy compressive loads. In the design life of a tall composite building, the building as well as CFST columns may be exposed to fire. The responses of loaded rectangular and circular CFST short and slender columns exposed to fire have been studied by many researchers experimentally [1-8] and numerically [9-15]. Standard fire tests indicated that the use of steel bar-reinforced concrete or fiber-reinforced concrete instead of plain concrete improved the fire performance of CFST columns. It was reported that CFST short columns of rectangular and square thin-walled sections failed by the outward local buckling coupled with concrete crushing while slender rectangular and square CFST columns failed by local and global interaction buckling. The air gap at the concrete-steel interface, concrete tensile strength, deformations induced by preloads, and local buckling have been shown to have marked influences on the structural responses of CFST columns to fire effects, which must be incorporated in the nonlinear fire response simulations of CFST columns to yield realistic fire resistance [12, 15].

After fire exposure, CFST columns in a composite building have been damaged in some degrees by fire effects, but they might not collapse. Therefore, the fire-damaged CFST columns must be repaired, which requires the assessment of their residual strength and stiffness in order to develop an economical solution to the post-fire repair. After being exposed to fire, the steel material could restore much of its strength while the strength of concrete has been significantly degraded [16]. Experiments could be conducted to determine the residual stiffness and strength of CFST columns after fire exposure. In a post-fire experiment, the CFST column is gradually loaded to failure in a room temperature environment [16-22]. Post-fire tests were performed on the residual strengths of rectangular and square CFST short and slender columns by Han et al. [16-18], circular CFST stub columns by Huo et al. [19], square and circular CFST slender columns by Rush et al. [20], and short CFST circular columns made of steel bar-reinforced concrete by Liu et al. [21, 22]. The post-fire experiments conducted by Han et al. [16] on rectangular CFST stub columns having the depth-to-thickness ratios of 35 and 45.5 indicted that these columns failed by the local buckling. In addition, increasing the exposure temperature resulted in earlier local-buckling of rectangular steel sections. Moreover, the maximum exposure temperature had a remarkable influence on the residual stiffness and strength of CFST columns. Han et al. [17] and Rush et al. [20] reported that slender square CFST columns failed by the local and global interaction buckling.

Although post-fire tests on CFST columns could be conducted, the tests are highly time-consuming and expensive. It is impossible to undertake post-fire tests on CFST columns in buildings to determine their residual strength and stiffness. Consequently, the assessment of the post-fire structural responses of CFST columns in buildings mainly relies on the use of nonlinear inelastic post-fire analysis techniques. Han et al. [16, 17] proposed analytical models for ascertaining the residual stiffness and strength of CFST short and slender columns after

exposure to elevated temperatures. The stress-strain laws of confined concrete at ambient temperature provided by Han et al. [23] were modified by using the expressions given by Li and Guo [24] for estimating the residual strength and strain of compressive concrete exposed to a maximum temperature and had cooled down to the room temperature. However, the outward local-buckling of thin-walled steel sections was not included in the analytical models presented by Han et al. [16, 17]. Yang et al. [25] proposed a finite element model using the fiber discretization for calculating the post-fire performance of loaded CFST slender columns. The finite element program ABAQUS was employed to investigate the residual strengths of short and slender CFST columns that considered various material and geometric parameters by Huo et al. [19], Liu et al. [21, 22], Song et al. [26], Yao and Hu [27] and Ibanez et al. [28].

The outward local-buckling of rectangular thin-walled steel sections, which markedly reduces the strength and stiffness of CFST columns with or without fire exposure [15, 16, 29-33], has not been considered in the existing theoretical models for post-fire simulations. To overcome this limitation, this paper presents a new fiber-based nonlinear post-fire simulation technique for quantifying the residual strength and stiffness of concentrically loaded short CFST column with rectangular thin-walled sections after exposure to fire accounting for progressive local buckling. The post-fire material laws for concrete in rectangular CFST columns are developed and incorporated in the proposed post-fire simulation model. The existing post-fire experimental results are utilized to verify the post-fire computer modeling procedure. A parametric study is performed that investigates the post-fire load-axial strain responses of thin-walled CFST stub columns after being exposed to high temperatures. A design formula is derived for estimating the residual strengths of CFST columns after being exposed to fire.

2. The fiber-based nonlinear post-fire simulation

2.1. Fiber element formulation

The present method of nonlinear post-fire analysis employs the fiber approach to mesh the cross-sections of rectangular CFST columns. The method of fiber analysis has shown to be an accurate and computationally efficient numerical technique for simulating the inelastic behavior of composite columns as it does not require the meshing of the column along its length [31-35]. The typical fiber mesh of a CFST column is shown in Fig. 2, in which the steel fiber size is equal to half of that of the concrete fiber. Each element in the cross-section represents either a steel fiber or a concrete fiber running longitudinally. The post-fire material properties can be assigned to steel and concrete fibers. The nonlinear post-fire simulation model is formulated by means of the following assumptions: (1) the CFST column has been exposed to elevated temperature; (2) the slip between the concrete core and steel tube in the longitudinal direction is zero; (3) the progressive local buckling of thin-walled steel sections is taken into account; (4) the shrinkage and creep of concrete are ignored. After fire exposure, the CFST column has been damaged in some degrees such as geometric damage of the steel tube. The geometric damage is represented by the initial geometric imperfection, which is considered in the effective width formulas of steel plates. The post-fire stress-strain models for steel and concrete are used to simulate the material behavior of damaged steel and concrete.

The strain compatibility requires that the steel tube and concrete in a CFST column loaded concentrically have the same axial strain. To determine the softening post-peak responses of CFST columns, the method of strain control is used in the computational procedure. In this method, the axial strain is gradually increased and the stresses in fiber elements are calculated from the given axial strain by means of employing the uniaxial material post-fire constitutive laws of concrete and steel. The numerical schemes given in Sections 2.4 and 2.5 are utilized to

model the post-local buckling in addition to the initial local-buckling of thin-walled steel sections and update the stresses of steel fibers in accordance with the effective width method. The internal axial force (P) is then computed by integrating the fiber stresses over the entire cross-section. By means of repeating the above computation process, the load-axial strain curve of the CFST stub column can be completely quantified. The incremental numerical analysis process is terminated when either the specified ultimate concrete strain is exceeded or the axial load falls to 50% of the column ultimate load [34].

2.2. Post-fire stress-strain laws for structural steels

The idealized elastic-plastic post-fire stress-strain curve with strain-hardening for structural steels given by Cheng [36] is shown in Fig. 3, which is implemented in the present nonlinear post-fire analysis technique. This stress-strain relationship of steel after exposure to elevated temperatures is expressed as

$$\sigma_s = \begin{cases} E_s \varepsilon_s & \text{for } \varepsilon_s \le \varepsilon_{yp} \\ f_{yp}(T) + E_{st}\left[\varepsilon_s - \varepsilon_{yp}(T)\right] & \text{for } \varepsilon_s > \varepsilon_{yp} \end{cases} \tag{1}$$

where σ_s , ε_s denote the longitudinal stress and strain in steel fibers, respectively; E_s the Young's modulus of steel that is exposed to room temperature, ε_{yp} the yield strain at post-fire, E_{st} the tangent modulus at strain hardening taken as $E_{st} = 0.01E_s$, T the maximum exposure temperature in °C, and f_{yp} the yield strength of structural steel after being exposed to elevated temperature and was given by Cheng [36] as

$$f_{yp} = \begin{cases} f_y & \text{for } T \le 400°C \\ f_y[1 + 2.33\times10^{-4}(T-20) - 5.88\times10^{-7}(T-20)^2] & \text{for } T > 400°C \end{cases} \quad (2)$$

in which f_y stands for the yield stress of steel at room temperature without exposure to elevated temperatures. Equation (2) is graphically represented in Fig. 4.

2.3. Post-fire stress-strain laws for concrete

The high temperatures significantly degrade the compressive strength of concrete. The available post-fire stress-strain models for concrete in CFST rectangular columns have been extremely limited due to the difficulty in testing the concrete in CFST columns after being exposed to fire. The stress-strain relationship for concrete at ambient temperature has been modified by utilizing the post-fire material properties of concrete and the modified model has been employed to model the material post-fire behavior of concrete in CFST columns by Han et al. [16] and Yang et al. [25]. In the present computer simulation technique, the stress-strain laws for compressive concrete at room temperature suggested by Mander et al. [37] are modified by using the post-fire material properties of concrete proposed by the authors in the present study to simulate the material responses of concrete in rectangular CFST columns after fire exposure as follows:

$$\sigma_{cp} = \frac{f_{cp}^{'}\lambda\left(\varepsilon_{cp}/\varepsilon_{cp}^{'}\right)}{\lambda - 1 + \left(\varepsilon_{cp}/\varepsilon_{cp}^{'}\right)^{\lambda}} \quad (3)$$

$$\lambda = \frac{E_{cp}}{E_{cp} - \left(f_{cp}^{'}/\varepsilon_{cp}^{'}\right)} \quad (4)$$

where σ_{cp} and ε_{cp} represent the post-fire concrete stress and strain in compression, respectively; $f_{cp}^{'}$ and $\varepsilon_{cp}^{'}$ the post-fire maximum compressive strength and corresponding strain of concrete, respectively; E_{cp} is the post-fire modulus of elasticity of concrete, which is calculated by the following equation given by ACI Committee 363 [38] with the post-fire compressive strength of concrete:

$$E_{cp} = 3320\sqrt{f_{cp}^{'}} + 6900 \ \ (\text{MPa}) \tag{5}$$

The post-fire maximum strength of compressive concrete in rectangular CFST columns and the corresponding strain were determined based on the experimental results on axially loaded short rectangular CFST columns tested by Han et al. [16]. In the computations of the post-fire maximum strengths of concrete in CFST columns, the post-fire steel yield strengths defined by Eq. (2) were used and the local buckling of steel sections was considered. The computed post-fire compressive strengths and corresponding strains of concrete in the tested CFST rectangular columns provided in Table 1 are presented in Figs. 5 and 6, respectively. Based on the nonlinear regressive analyses, expressions for determining the post-fire maximum compressive strength and corresponding strain of concrete in rectangular CFST columns are proposed by the authors herein as follows:

$$f_{cp}' = \left(-6\times10^{-7}T^2 - 2\times10^{-4}T + 0.952\right) f_c' \tag{6}$$

$$\varepsilon_{cp}' = \left(2.14\times10^{-6}T^2 + 3.66\times10^{-3}T + 1\right)\varepsilon_c' \tag{7}$$

in which T is the maximum temperature to which the CFST column has been exposed; $f_c^{'}$ and

ε_c' the compressive strength and corresponding strain of the concrete cylinder at room temperature. It should be noted Eqs. (6) and (7) have been proposed based on experimental results on CFST columns with $f_c^{'} \le 55$ MPa. The strain ε_c' of concrete at room temperature can be computed by the following expressions suggested by Liang [31]:

$$\varepsilon_c^{'} = \begin{cases} 0.002 & \text{for } f_c^{'} \le 28 \text{ MPa} \\ 0.002 + \dfrac{f_c^{'} - 28}{54000} & \text{for } 28 < f_c^{'} \le 82 \text{ MPa} \\ 0.003 & \text{for } f_c^{'} > 82 \text{ MPa} \end{cases} \tag{8}$$

The post-fire compressive strengths and corresponding strains of concrete in rectangular CFST columns calculated by the proposed Eqs. (6) and (7) are compared with those obtained from the experiments conducted by Han et al. [16] in Figs. 5 and 6, respectively. The figures demonstrate that the proposed formulas predict well the post-fire compressive strengths and corresponding strains of concrete. The typical post-fire stress-strain curves of concrete in CFST columns with rectangular steel sections based on the proposed material constitutive models are presented in Fig. 7.

2.4. Modeling of initial local buckling

After exposure to high temperatures, the steel tube in a CFST column with rectangular thin-walled section loaded gradually at ambient temperature will undergo the progressive outward local buckling from the onset of initial local buckling to the post-local buckling. Kamil et al. [33] proposed equations for the calculations of the initial local-buckling stress of steel plates subjected to stress gradients in rectangular CFST columns exposed to room temperature as well as elevated temperatures. When a steel plate has been cooled down from elevated temperatures,

it can restore much of its strength. For the post-fire analysis, the CFST column has been cooled down to the room temperature so that the equations developed by Kamil et al. [33] for thin steel plates at ambient temperature can be applied to the determination of the initial local-buckling stress of the steel tube walls in the CFST column after fire exposure. This can be done by means of replacing the yield strength of steel at room temperature with its post-fire yield strength.

The critical stress ($\sigma_{1c,p}$) that causes the initial local buckling of the thin-walled steel walls in a CFST column subjected to uniform compression after fire exposure can be calculated by the following equation given by Kamil et al. [33]:

$$\frac{\sigma_{1c,p}}{f_{yp}} = (g_1 \lambda_{c,p}^{g} + g_2) \frac{0.6566 \lambda_{c,p}^{0.001521}}{0.5415 \lambda_{c,p}^{4.889} + 1} \tag{9}$$

where $\lambda_{c,p}$ stands for the relative slenderness ratio of the column cross-section at the post-fire, expressed by

$$\lambda_{c,p} = \sqrt{\frac{12(1-\nu^2)(b/t_s)^2 f_{yp}}{k\pi^2 E_s}} \tag{10}$$

where *b*, t_s are the clear width and thickness of steel section, respectively; ν the Poisson's ratio of steel; and *k* the coefficient for the elastic local buckling of clamped plates, taken as 9.95 [33].

The coefficients g, g_1 and g_2 in Eq. (9) are calculated by

$$g = -7.9339\alpha_s^2 + 11.29\alpha_s + 4.701 \tag{11}$$

$$g_1 = 0.0863\alpha_s^2 - 0.1248\alpha_s + 0.0431 \tag{12}$$

$$g_2 = 0.2656\alpha_s^2 - 0.9902\alpha_s + 1.719 \tag{13}$$

In Eqs. (11) to (13), α_s is the stress-gradient coefficient, which is equal to 1.0 for a steel plate subjected to uniform edge compressive stresses. It should be noted that Eq. (9) is applicable to steel tube walls in a CFST column with a clear width-to-thickness ratio in the range of $30 \le b/t_s \le 100$.

2.5. Modeling of post-local buckling

The method of effective width is usually employed to determine the post-local buckling strengths of thin steel plates that fabricate a rectangular CFST column [30, 31, 34]. Figure 8 illustrates the ineffective and effective widths of a rectangular steel cross-section filled with concrete subjected to axial compression. Kamil et al. [33] proposed effective width formulas for calculating the strengths of post-local buckling of thin steel plates exposed to various temperatures. Their formulas are incorporated in the fiber-based post-fire model to ascertain the effective widths of steel sections in CFST columns after fire exposure, which are written as

$$\frac{b_e}{b} = (q_1\lambda_{c,p}^{q})\frac{0.8418\lambda_{c,p}^{0.02368} + 1.154}{2.055 + \lambda_{c,p}^{1.68}} \tag{14}$$

in which b_e denotes the effective width of a steel tube wall depicted in Fig. 8, and q and q_1 are expressed as

$$q = 0.04007\alpha_s^2 - 0.05275\alpha_s + 0.03355 \tag{15}$$

$$q_1 = 0.1007\alpha_s^2 - 0.7027\alpha_s + 1.65 \quad (16)$$

It should be noted that Eq. (14) is applicable to steel tube walls in a CFST column with a clear width-to-thickness ratio in the range of $30 \le b/t_s \le 100$. The method of effective width assumes that steel fibers within the effective widths are stressed to the yield strength of the steel material while steel fibers within the ineffective widths withstand zero stress. This method determines the ultimate strength of a thin steel plate under compression. A thin steel plate has the capacity of undergoing the progressive buckling from initial local buckling to the post-local buckling until attains its ultimate limit state. In this gradual buckling process, the in-plane stresses in the heavily buckled regime are redistributed to the edge strips of the plate [34]. After the onset of initial local bulking, the ineffective width of the steel plate increases with increasing the loading until its ultimate strength is attained. The computer modeling technique developed by Liang [31] is adopted in the post-fire analysis procedure to model the gradual post-local buckling of steel sections after fire exposure.

3. Experimental verification

The post-fire ultimate loads of rectangular and square CFST short columns obtained by the computational model are compared against experimentally measured data given by Han et al. [16, 39] to verify its accuracy. The details of the CFST columns tested are listed in Table 1. It is seen from Table 1 that the D/t_s ratio of square sections was 20 while rectangular sections had the D/t_s ratio of 43. Therefore, the local buckling of rectangular CFST columns shown in Table 1 was considered in the nonlinear post-fire analysis. It is noted that the cross-sectional dimensions of all columns listed in Table 1 are smaller than those of concrete cubes that were

employed to estimate the compressive strength of concrete in tested specimens. As a result of this, the actual compressive strength of concrete in these specimens was conservatively taken as the average compressive strength of concrete cubes in the post-fire simulations of these columns. The predicted post-fire ultimate axial strengths ($P_{u.fib}$) of CFST columns and corresponding experimentally measured values ($P_{u.\exp}$) are given in Table 1. The comparison indicates that good agreement between predictions and experimental data is generally obtained. The mean value of the $P_{u.fib}/P_{u.\exp}$ ratios is 0.961. The discrepancy between the theory and post-fire tests is likely caused by the fact that the measurements on the post-fire stress-strain relations for concrete and steel were not undertaken and might be different from those implemented in the computer model.

The predicted post-fire load-axial strain responses of Specimens S-20-1, S-200, S-300, S-600, S-800, S900, R2-200, R2-400, R2-800 and R2-900 are compared with experimentally measured data reported by Han et al. [16, 39] in Figs. 9 and 10. It would appear that the experimental post-fire load-axial strain responses of square CFST short columns are captured reasonably well by the nonlinear post-fire simulation technique. It is confirmed that the post-peak responses of CFST columns after being exposed to temperatures up to 400 ^{o}C are characterized by the descending load-strain behavior while columns after being exposed to temperatures higher than 400 ^{o}C experience strain-hardening behavior in the post-yield regime.

4. Post-fire behavior of CFST columns

The nonlinear post-fire modeling technique proposed was utilized to examine the significance of the outward local buckling, concrete strength, steel yield strength and the width-to-thickness ratio on the post-fire structural behavior of short CFST columns with thin-walled rectangular

sections. In the parametric studies, the modulus of elasticity of steel at room temperature was specified as 210 GPa. The effect of local buckling was taken into consideration in the nonlinear post-fire analyses of CFST columns having clear width-to-thickness ratios ranging from 30 to100.

4.1. Effects of local buckling

The nonlinear post-fire simulation technique proposed was used to examine the significance of the outward local buckling on the post-fire ultimate strengths of stub CFST columns. For this purpose, square steel columns with 500×500 mm, the B / t_s ratio of 100, and yield strength of 300 MPa filled with 40 MPa concrete were analyzed by means of including and excluding local buckling, respectively. These columns had been exposed to the maximum temperatures ranging from 20 °C to 800 °C and cooled down to the ambient temperature. The post-fire load-axial strain curves of the CFST columns after exposure to the temperature of 600 °C have been plotted in Fig. 11. It is demonstrated that the load-strain curve computed by considering local buckling departs from the one without considering local buckling. The local buckling causes a significant reduction in the column ultimate load by 14% after being exposed to 600 °C temperature. Figure 12 provides the column strength-maximum exposure temperature curves. The figure demonstrates that the strength reduction caused by local buckling increases as the maximum exposure temperature rises. The percentage reductions in the ultimate loads of CFST columns due to local buckling after being heated to 400 °C, 700° C and 800 °C are 12%, 16% and 18%, respectively. It would appear that local buckling causes more reductions in the ultimate strengths of CFST columns after exposure to high temperatures in comparison with CFST columns without exposure to fire [32]. This is mainly caused by the fact that after being cooled down from an elevated temperature, the steel can restore an immense magnitude of its

strength while the concrete suffers a sustainable degradation in its strength. Consequently, the contribution of steel tube after fire exposure to the column strength is relatively more than that of the one without fire exposure due to the lower post-fire concrete strength.

4.2. Effects of concrete strength

The sensitivities of the post-fire responses of CFST rectangular columns to the concrete compressive strength were examined by conducting nonlinear fiber analyses on the steel columns of 500×600×6 mm filled with concrete having compressive strengths ranging from 25 MPa to 55 MPa. The yield stress of steel tubes at room temperature was 350 MPa. The calculated post-fire load-axial strain responses of the CFST columns after being heated to the temperature of 600°C are given in Fig. 13. It is illustrated that the column initial axial stiffness is not sensitive to the change of concrete strength, but at higher load levels, increasing the concrete strength leads to a remarkable improvement in the column axial stiffness. The post-fire column ultimate load is shown to have a significant increase when increasing the concrete strength. Figure 14 depicts the significance of concrete strength on the column strength-maximum exposure temperature curves. Increasing the concrete strength markedly improves the column ultimate load, but this effect decreases when rising the maximum exposure temperature. When changing the concrete strength from 25 MPa to 35 MPa, 45 MPa and 55 MPa after being heated to the temperature of 400 °C, the percentage increases in the column ultimate load are 27%, 53% and 80%, respectively. After the columns were heated to the temperature of 600 °C, however, the column ultimate load is reduced by 25%, 50% and 75%, respectively, if the concrete strength is changed from 25 MPa to 35 MPa, 45 MPa and 55 MPa.

4.3. Effects of steel yield strength

The post-fire simulation model was employed to analyze rectangular CFST columns fabricated by thin-walled steel tubes with yield strengths varying from 250 MPa to 450 MPa. The columns under investigation had the cross-sectional dimensions of 450×550×10 mm and a B / t_s ratio of 45 and were constructed by concrete with compressive strength of 45 MPa. The post-fire load-axial strain responses of these columns with various steel yield strengths after being exposed to the temperature of 600 °C have been plotted in Fig. 15. It is clearly demonstrated that the column initial stiffness is not affected by the steel yield strength. The higher of the steel yield strength, the higher of the post-fire ultimate load of the CFST column. Figure 16 gives the post-fire ultimate strengths of CFST columns that were made of steel tubes having different yield strengths after being experienced different temperatures. It is discovered that using steel tubes with higher yield strength results in a considerable increase in the column strength regardless of the exposure temperature. However, the effect of steel yield strength on the column post-fire ultimate load is shown to increase with rising the exposure temperature. After exposure to the temperature of 400 °C, changing the steel yield strength from 250 MPa to 300 MPa, 350 MPa and 450 MPa leads to the increase in the column post-fire strength by 6%, 11% and 22%, respectively; if the columns were exposed to the temperature of 800 °C, the corresponding strength increase is 8%, 16% and 31%, respectively.

4.4. Effects of width-to-thickness ratio

The B / t_s ratio has a marked influence on the post-fire strengths of CFST columns. To investigate this effect, the computer model was utilized to analyze square CFST columns that had the cross-section of 600×600 mm. The B / t_s ratios of 40, 60, 80 and 100 were determined by varying only the thickness of the steel tubes. The steel yield strength of 350 MPa and the concrete compressive strength of 35 MPa were specified in the analyses. Figure 17 depicts the

post-fire load-axial strain curves for CFST columns after exposure to 700 °C temperature. It is clearly shown that the use of a larger B/t_s ratio in CFST columns leads to a remarkable reduction in the column post-fire initial axial stiffness. The relationships between the column post-fire strength, the maximum exposure temperature and the B/t_s ratio are explicitly illustrated in Fig. 18. The computational solutions indicate that increasing the B/t_s ratio greatly decreases the column post-fire ultimate loads for all levels of exposure temperatures. However, the influence of the B/t_s ratio on the post-fire ultimate load increases as the exposure temperature rises. When changing the B/t_s ratio from 40 into 60, 80 and 100 for CFST columns being exposed to the temperature of 600 °C, the reduction in the post-fire ultimate load is 22%, 33% and 40%, respectively; for columns being heated to the temperature of 800 °C, however, the strength reduction is 25%, 37% and 45%, respectively. This implies that the larger the B/t_s ratio and the higher exposure temperature, the greater reduction in the column post-fire strength.

5. Proposed design formula

Although the computer post-fire simulation technique developed can be used directly in the assessment of the residual stiffness and strength of CFST columns after being exposed to fire, a simple design formula is needed for use in design practice. The design formula for estimating the post-fire ultimate axial load of rectangular CFST short columns loaded concentrically is proposed herein as

$$P_u = A_{se} f_{yp} + A_c f'_{cp} \tag{17}$$

where P_u is the post-fire ultimate axial load of the short CFST column, A_{se} the effective cross-sectional area of the steel section that is computed by Eq. (14), and A_c the cross-sectional area of the concrete infill. Equation (17) is applicable to CFST short columns with $L/D \le 3$, a clear width-to-thickness ratio in the range of $30 \le b/t_s \le 110$ and concrete with $f_c' \le 55$ MPa.

The post-fire ultimate axial loads of CFST columns calculated by the proposed formula are compared against experimental data in Table 1, where $P_{u,cal}$ is the column ultimate axial strength computed by the proposed Eq. (17). It can be observed from Table 1 that the calculated results are in good agreement with test data. The mean value of $P_{u,cal}/P_{u,\exp}$ ratios is 0.941. The statistical analysis shows that the standard deviation is 0.055 and the coefficient of variation is 0.058. The proposed design formula generally yields conservative results compared with the computer simulation model. This is due to the fact that the post-fire steel yield strength was used in the simple calculations while the computer simulation model considered the strain-hardening of steel. The comparative study shows that the simple design formula proposed can be used in practice to assess the residual strengths of fire-damaged thin-walled CFST columns.

6. Design example

A design example is presented herein to demonstrate the design procedure using the proposed design equations for determining the post-fire ultimate axial strength of CFST short columns after being exposed to fire. The square CFST short column with cross-section of 500×500 mm and thickness of 10 mm is considered. The concrete design strength f_c' is 45 MPa and the steel yield strength f_y is 350 MPa at ambient temperature. The column has been exposed to the steady state temperature of 600 °C and cooled down to the room temperature.

Solution:

The post-fire yield strength of steel is calculated as

$$\begin{aligned} f_{yp} &= f_y[1+2.33\times10^{-4}(T-20)-5.88\times10^{-7}(T-20)^2] \\ &= 350\times[1+2.33\times10^{-4}\times(600-20)-5.88\times10^{-7}\times(600-20)^2] \\ &= 328.06 \text{ MPa} \end{aligned}$$

The post-fire compressive strength of concrete is computed as

$$\begin{aligned} f'_{cp} &= \left(-6\times10^{-7}T^2-2\times10^{-4}T+0.952\right)f'_c \\ &= \left(-6\times10^{-7}\times600^2-2\times10^{-4}\times600+0.952\right)\times45 \\ &= 27.72 \text{ MPa} \end{aligned}$$

The effective area of the steel tube is determined as follows:

$$\begin{aligned} \frac{b_e}{b} &= (q_1\lambda_{c,p}^q)\frac{0.8418\lambda_{c,p}^{0.02368}+1.154}{2.055+\lambda_{c,p}^{1.68}} \\ &= \left[1.048\times(0.633)^{0.2087}\right]\times\frac{0.8418\times(0.633)^{0.02368}+1.154}{2.055+(0.633)^{1.68}} \\ &= 0.8187 \\ \therefore\ b_e &= 0.8187\times480 = 392.98 \text{ mm.} \end{aligned}$$

The total effective area of the steel tube is $A_{se} = 16119.2$ mm^2

The post-fire ultimate axial load of the column is therefore

$$\begin{aligned} P_u &= A_{se}f_{yp}+A_cf'_{cp} \\ &= 16119.2\times328.06+230400\times27.72 \text{ N} = 11674.75 \text{ kN.} \end{aligned}$$

7. Conclusions

A fiber-based nonlinear post-fire simulation technique has been described in this paper, which calculates the post-fire structural responses of concentrically loaded short CFST columns of

rectangular thin-walled sections after being exposed to high temperatures. The computational model for post-fire simulations of CFST columns has incorporated the important feature of the progressive local and post-local buckling of non-compact and slender steel sections, which has not been included in other theoretical post-fire models. The post-fire stress-strain models for concrete in rectangular CFST columns has been proposed based on experimental data and have been used in the numerical studies. The proposed post-fire modeling technique generally gives good predictions of the post-fire responses of short CFST columns loaded concentrically. The post-fire behavior of short rectangular CFST columns with various parameters has been studied by utilizing the computer simulation program developed. A design formula has been proposed for quantifying the post-fire ultimate strengths of axially loaded short CFST rectangular columns considering post-local buckling.

The concluding remarks are provided as follows:

(1) The outward local buckling markedly reduces the post-fire ultimate loads of CFST columns fabricated with rectangular thin-walled sections, and its effect increases as the maximum exposure temperature increases.

(2) Using high strength concrete greatly improves the post-fire ultimate strength of CFST short columns, but its influence decreases when the maximum exposure temperature rises. The steel tube completely encases the filled high-strength concrete, which considerably improves the concrete ductility and prevents the spalling of high strength concrete.

(3) The post-fire ultimate load of CFST columns is increased considerably by means of using higher yield strength steel tubes. The influence of steel yield strength increases as the exposure temperature increases.

(4) Increasing the B/t_s ratio sustainably decreases the post-fire stiffness and strength of CFST columns, and its influence increases when increasing the exposure temperature.

(5) The design formula proposed is demonstrated to give good prediction of the post-fire ultimate strengths of CFST columns.

References

[1] T.T. Lie and M. Chabot, Experimental studies on the fire resistance of hollow steel columns filled with plain concrete, Internal report, National Research Council Canada, Institute for Research in Construction, 1992-01.

[2] Y. Sakumoto, T. Okada, M. Yoshida and S. Tasaka, Fire resistance of concrete-filled, fire-resistant steel-tube columns, J. Mat. in Civil Eng. ASCE 69 (2) (1994) 169-184.

[3] V.K.R. Kodur and T.T. Lie, Fire performance of concrete-filled hollow steel columns, J. Fire Prot. Eng. 79 (3) (1995) 89-98.

[4] L.H. Han, Y.F. Yang and L. Xu, An experimental study and calculation on the fire resistance of concrete-filled SHS and RHS columns, J. Constr. Steel Res. 59 (2003) 427-452.

[5] D.K. Kim, S.M. Choi, J.H. Kim, K.S. Chung and S.H. Park, Experimental study on fire resistance of concrete-filled steel tube column under constant axial loads, J. Steel Struct. 5 (4) (2005) 305-313.

[6] A. Espinos, M.L. Romero, E. Serra and A. Hospitaler, Experimental investigation on the fire behavior of rectangular and elliptical slender concrete-filled tubular columns, Thin-Walled Struct. 93 (2015) 137-148.

[7] L.H. Han, F. Chen, F.Y. Liao, Z. Tao and B. Uy, Fire performance of concrete filled stainless steel tubular columns, Eng. Struct. 56 (2013) 165-181.

[8] Y.F. Yang, L. Zhang and X. Dai, Performance of recycled aggregate concrete-filled square steel tubular columns exposed to fire, Adv. in Struct. Eng. 20 (9) (2017) 1340-1356.

[9] T.T. Lie and R.J. Irwin, Fire resistance of rectangular steel columns filled with bar-reinforced concrete, J. Struct. Eng. ASCE 12 (5) (1995) 797-805.

[10] L.H. Han, Fire performance of concrete filled steel tubular beam-columns, J. Constr. Steel Res. 57 (2001) 695-709.

[11] K. Chung, S. Park and S. Choi, Material effect for predicting the fire resistance of concrete-filled square steel tube column under constant axial load, J. Constr. Steel Res. 64 (2008) 1505-1515.

[12] J. Ding and Y.C. Wang, Realistic modelling of thermal and structural behaviour of unprotected concrete filled tubular columns in fire, J. Constr. Steel Res. 64 (2008) 1086-1102.

[13] A. Espinos, M.L. Romero and A. Hospitaler, Advanced model for predicting the fire response of concrete filled tubular columns, J. Constr. Steel Res. 66 (2010) 1030-1046.

[14] S.D. Hong and A.H. Varma, Analytical modeling of the standard fire behavior of loaded CFT columns, J. Constr. Steel Res. 65 (2009) 54-69.

[15] G.M. Kamil, Q.Q. Liang and M.N.S. Hadi, Numerical analysis of axially loaded rectangular concrete-filled steel tubular short columns at elevated temperatures, Eng. Struct. 180 (2018) 89-102.

[16] L.H. Han, H. Yang and S.L. Cheng, Residual strength of concrete filled RHS stub columns after exposure to high temperatures, Adv. in Struct. Eng. 5 (2002) 123-133.

[17] L.H. Han and J.S. Huo, Concrete-filled structural steel columns after exposure to ISO-834 fire standard, J. Struct. Eng. ASCE 129 (1) (2003) 68-78.

[18] L.H. Han, J.S. Huo and Y.C. Wang, Compressive and flexural behavior of concrete filled steel tubes after exposure to standard fire, J. Constr. Steel Res. 61 (2005) 882-901.

[19] J. Huo, G. Huang and Y. Xiao, Effects of sustained axial load and cooling phase on post-fire behavior of concrete-filled steel tubular stub columns, J. Constr. Steel Res. 65 (2009) 1664-1676.

[20] D.I. Rush, L. Bisby, A. Jowsey and B. Lane, Residual capacity of fire-exposed concrete-filled steel hollow section columns, Eng. Strucut. 100 (2015) 550-563.

[21] F. Liu, L. Gardner and H. Yang, Post-fire behaviour of reinforced concrete stub columns confined by circular steel tubes, J. Constr. Steel Res. 102 (2014) 82-103.

[22] F. Liu, H. Yang and L. Gardner, Post-fire behaviour of eccentrically loaded reinforced concrete columns confined by circular steel tubes, J. Constr. Steel Res. 122 (2016) 495-510.

[23] L.H. Han, X.L. Zhao and Z. Tao, Tests and mechanics model of concrete-filled SHS stub columns, columns and beam-columns, Steel and Comp. Struct. 1 (1) (2001) 51-74.

[24] W. Li and Z.H. Guo, Experimental investigation of strength and deformation of concrete at elevated temperatures, Build. Struct. 14 (1) (1993) 8-16 (in Chinese).

[25] H. Yang, L.H. Han and Y.C. Wang, Effects of heating and loading histories on post-fire cooling behaviour of concrete-filled steel tubular columns, J. Constr. Steel Res. 64 (5) (2008) 556-570.

[26] T.Y. Song, L.H. Han and H.X. Yu, Concrete filled steel tube stub columns under combined temperature and loading, J. Constr. Steel Res. 66 (2010) 369-384.

[27] Y. Yao and X.X. Hu, Cooling behavior and residual strength of post-fire concrete filled steel tubular columns, J. Constr. Steel Res. 112 (2015) 282-292.

[28] C. Ibanez, L. Bisby, D. Rush, M.L. Romero and A. Hospitaler, Analysis of concrete-filled steel tubular columns after fire exposure, The 12th Int. Conf. on Adv. in Steel-Concrete Compos. Struct. (2018) 795-802.

[29] Q.Q. Liang, B. Uy and J.Y.R. Liew, Nonlinear analysis of concrete-filled thin-walled steel box columns with local buckling effects, J. Constr. Steel Res. 62 (2006) 581-591.

[30] Q.Q. Liang, B. Uy and J.Y.R. Liew, Local buckling of steel plates in concrete-filled thin-walled steel tubular beam-columns, J. Constr. Steel Res. 63 (3) (2007) 396-405.

[31] Q.Q. Liang, Performance-based analysis of concrete-filled steel tubular beam-columns. Part I: Theory and algorithms, J. Constr. Steel Res. 65 (2) (2009) 363-373.

[32] Q.Q. Liang, Performance-based analysis of concrete-filled steel tubular beam–columns, Part II: Verification and applications, J. Constr. Steel Res. 65 (2) (2009) 351-362.

[33] G.M. Kamil, Q.Q. Liang and M.N.S. Hadi, Local buckling of steel plates in concrete-filled steel tubular columns at elevated temperatures, Eng. Struct. 168 (2018) 108-118.

[34] Q.Q. Liang, Analysis and design of steel and composite structures, Boca Raton and London: CRC Press, Taylor and Francis Group; 2014.

[35] Q.Q. Liang, Nonlinear analysis of circular double-skin concrete-filled steel tubular columns under axial compression, Eng. Struct. 131 (2017) 639-650.

[36] S.L. Cheng, Behvaiors of concrete-filled rectangular steel tubes subjected to axial compression after high temperatures, ME Thesis, School of Civil Engineering, Harbin Institute of Technology, Harbin, China (in Chinese).

[37] J.B. Mander, M.N.J. Priestly and R. Park, Theoretical stress-strain model for confined concrete, J Struct. Eng. ASCE 114 (8) (1998) 1804-1826.

[38] ACI Committee 363, Sate of the Art Report on High-Strength Concrete, ACI Publication 363R-92, Detroit, MI: American Concrete Institute, 1992.

[39] L.H. Han, H. Yang and S.L. Chen, Tests on the residual strength of concrete filled steel tubes after high temperatures, Proc. of the First Int. Conf. on Steel and Compos. Struct. Pusan, Korea, 14-16 June 2001; 1709-1716.

Kamil, G. M., Liang, Q. Q. and Hadi, M. N. S. (2019). Nonlinear post-fire simulation of concentrically loaded rectangular thin-walled concrete-filled steel tubular short columns accounting for progressive local buckling. *Thin-Walled Structures*, 145: 106423.

Figures and Tables

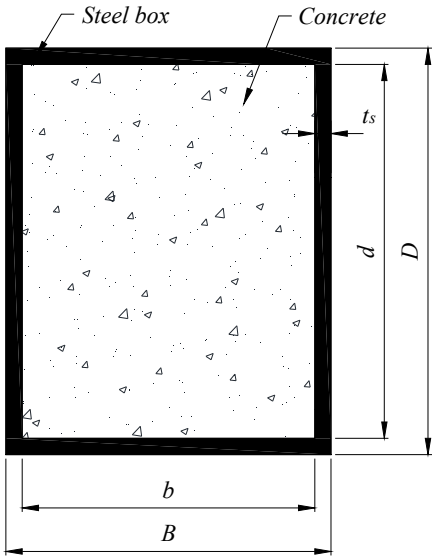

Fig. 1. Cross-section of rectangular CFST column.

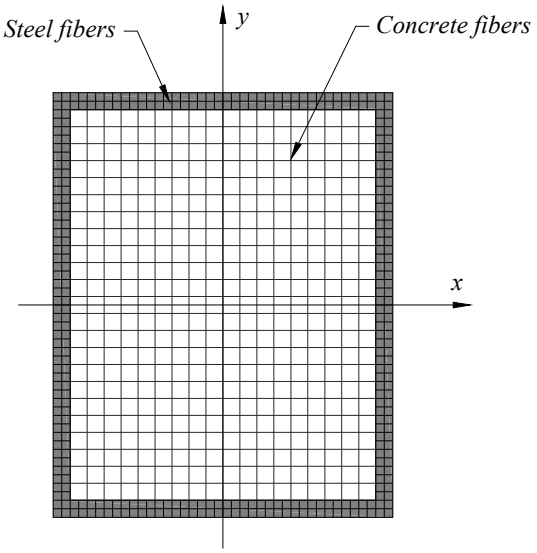

Fig. 2. Typical fiber element discretization.

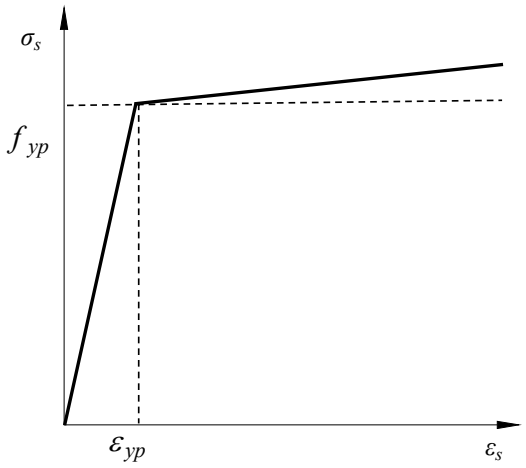

Fig. 3. Idealized post-fire stress-strain curve for structural steels.

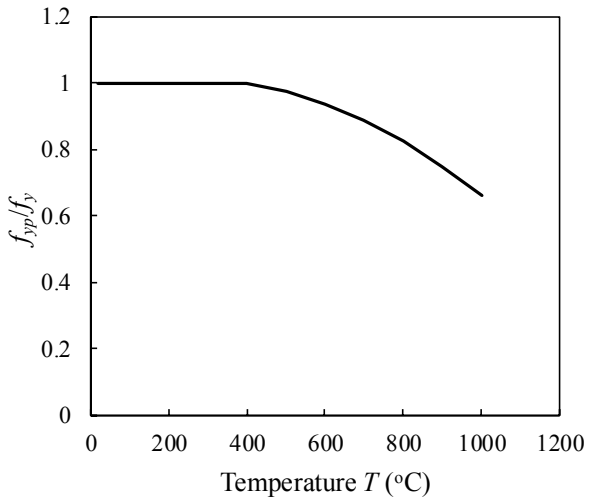

Fig. 4. Post-fire steel yield strength-temperature curve.

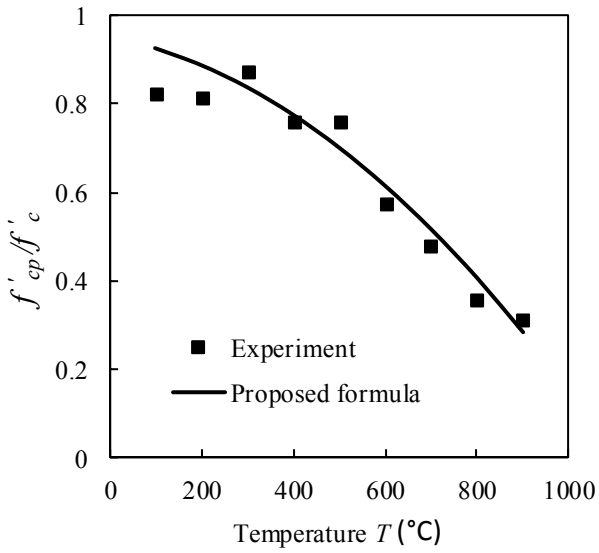

Fig. 5. Comparison of the post-fire maximum compressive strengths of concrete in rectangular CFST columns obtained from experiments and by the proposed formula.

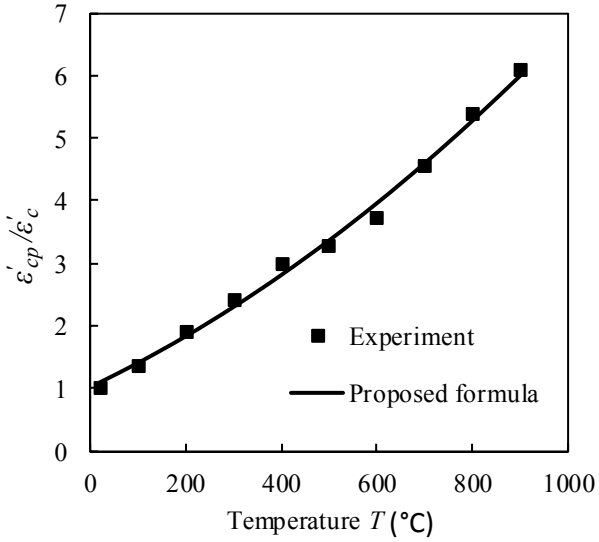

Fig. 6. Comparison of the post-fire strains ε'_{cp} of concrete in rectangular CFST columns obtained from experiments and by the proposed formula.

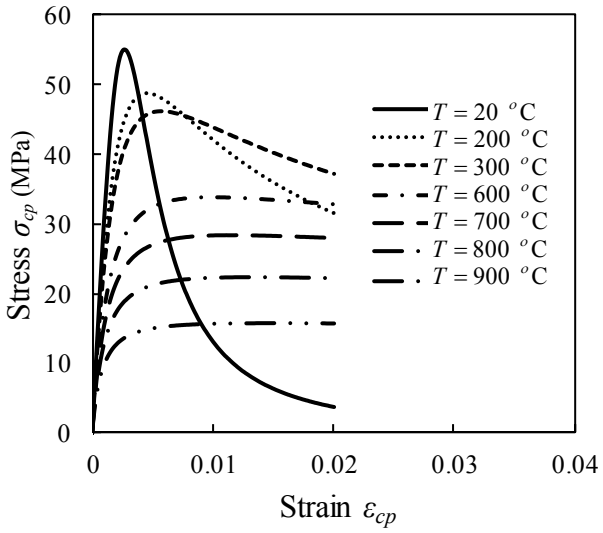

Fig. 7. Typical post-fire stress-strain curves for concrete in rectangular CFST columns.

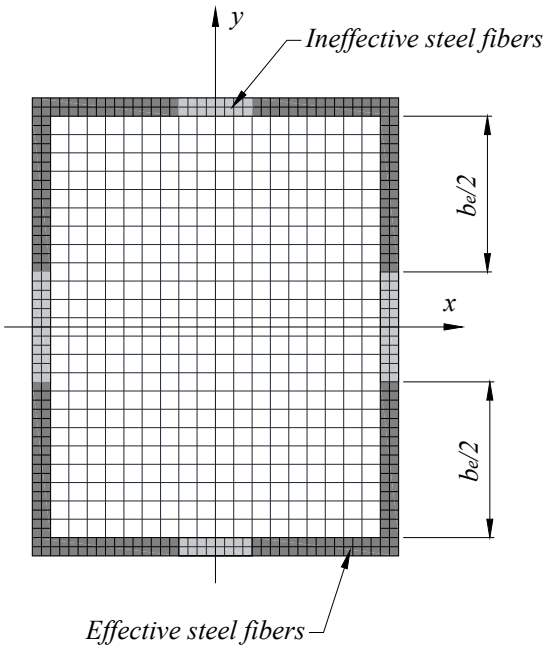

Fig. 8. Effective widths of steel tube walls in rectangular CFST column section.

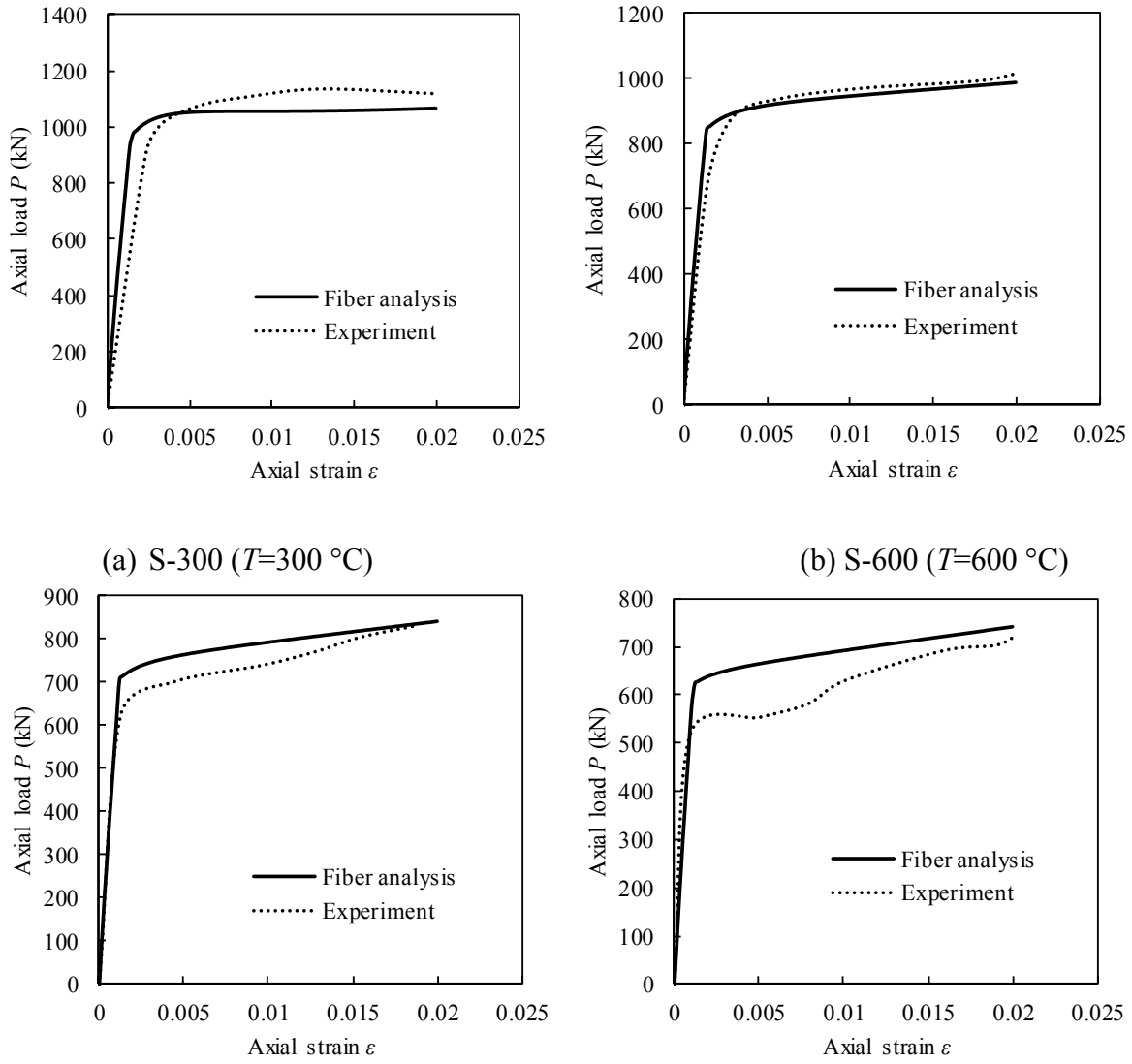

Fig. 9. Comparison of predicted and experimental post-fire axial load-strain responses of square CFST columns after exposure to high temperatures.

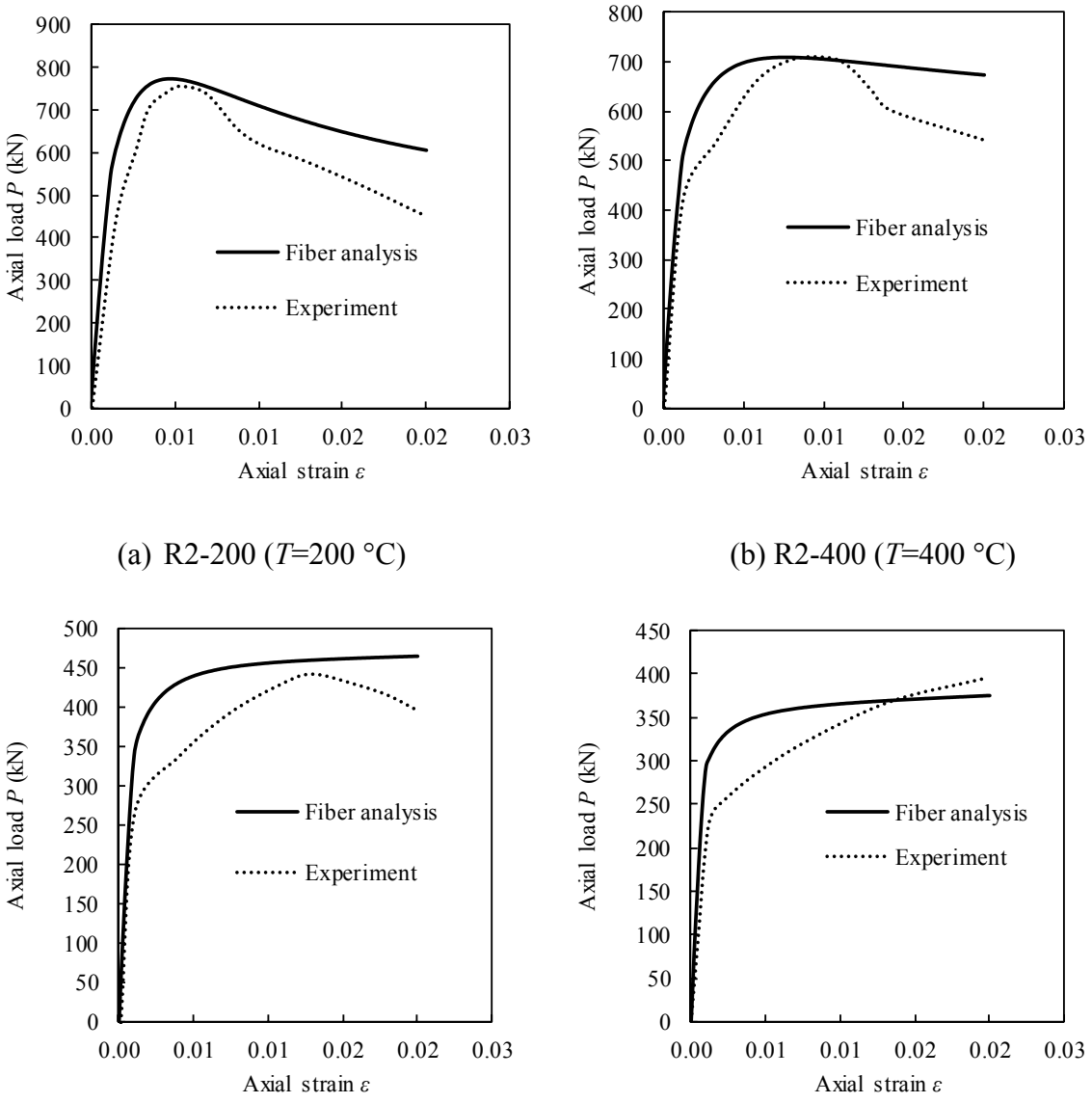

Fig. 10. Comparison of predicted and experimental post-fire axial load-strain responses of rectangular CFST columns after exposure to high temperatures.

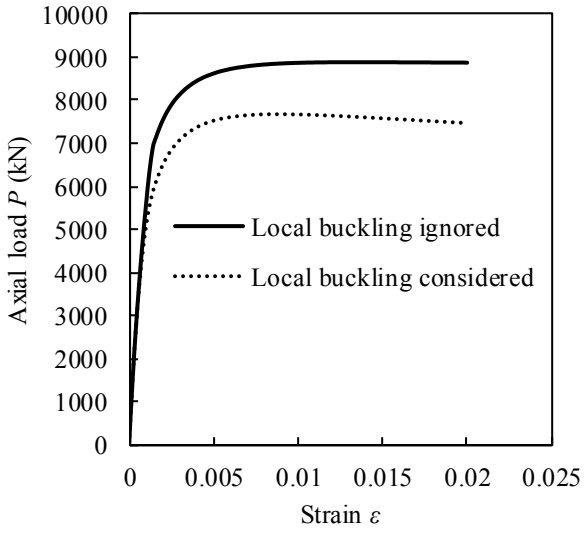

Fig. 11. Influences of local buckling on the post-fire axial load-strain behavior of square CFST column after being exposed to temperature of 600 °C.

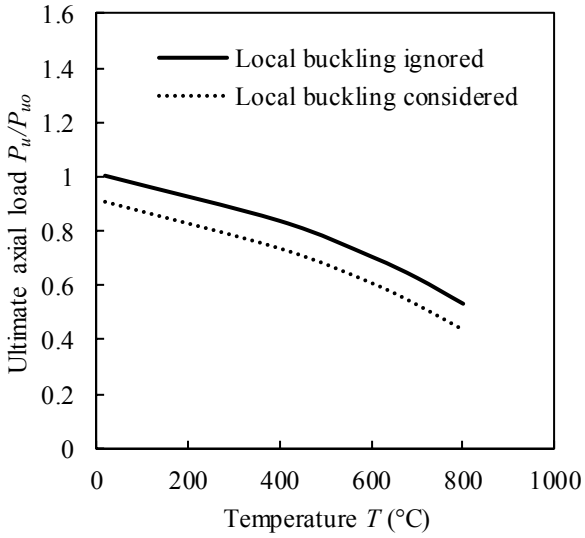

Fig. 12. Influences of local buckling on the post-fire ultimate axial strengths of square CFST column.

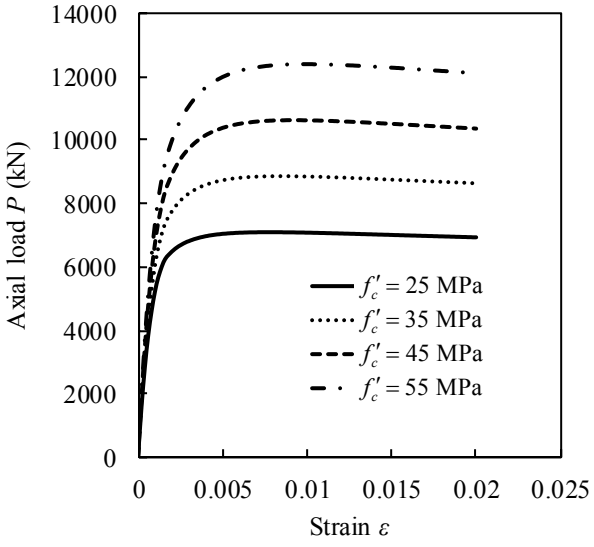

Fig. 13. Post-fire axial load-strain curves of rectangular CFST columns with various concrete strengths after being exposed to temperature of 600 °C.

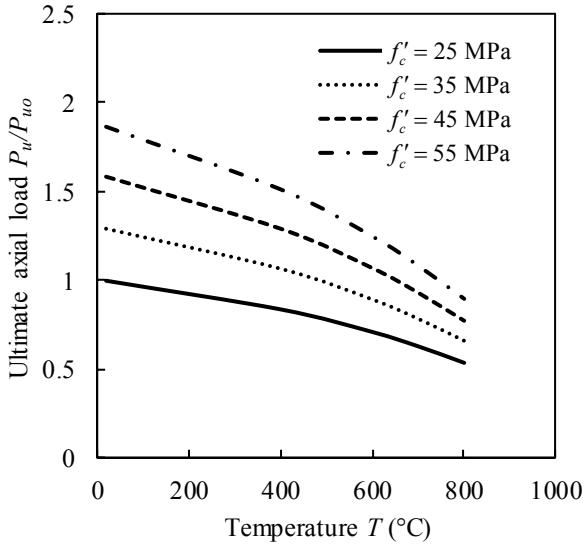

Fig. 14. Effects of concrete strength on the post-fire ultimate strength-exposure temperature curves for rectangular CFST columns.

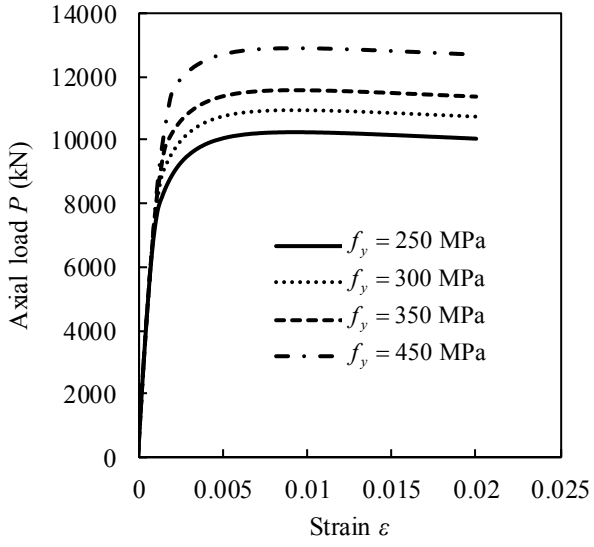

Fig. 15. Effects of steel yield strength on the post-fire axial load-strain curves of rectangular CFST columns after being exposed to temperature of 600 °C.

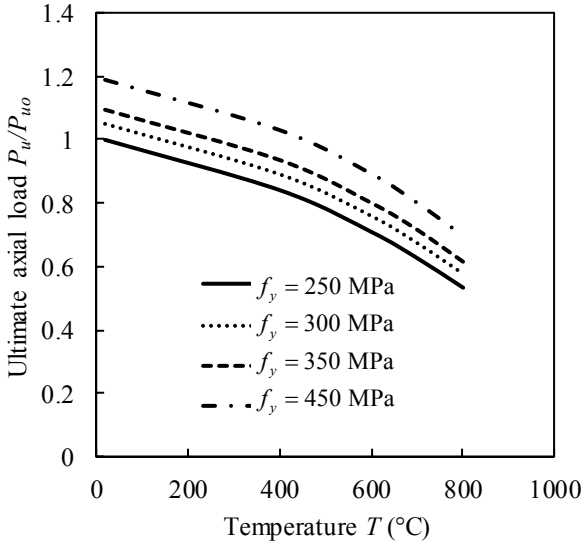

Fig. 16. Effects of steel yield strength on the post-fire ultimate strength-exposure temperature curves for rectangular CFST columns.

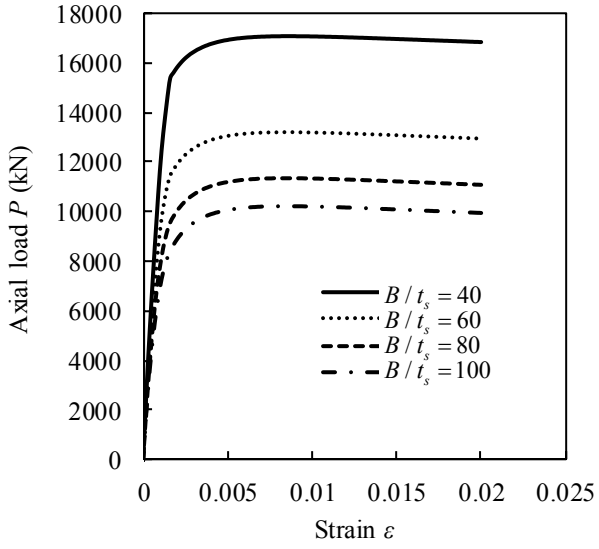

Fig. 17. Effects of B/t_s ratios on the post-fire axial load-strain responses of square CFST columns after being exposed to temperature of 600 °C.

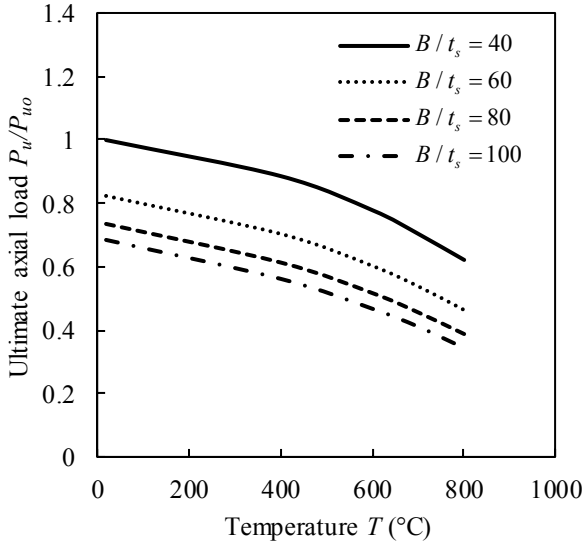

Fig. 18. Effects of B/t_s ratios on the post-fire ultimate strength-exposure temperature curves for square CFST columns.

Table 1. Post-fire ultimate axial loads of rectangular and square CFST short columns under axial compression

Specimen	T (°C)	$B\times D\times t_s$ (mm)	L (mm)	f_y (MPa)	f_{cu} (MPa)	$P_{u,\exp}$ (kN)	$P_{u,fib}$ (kN)	$P_{u,cal}$ (kN)	$\frac{P_{u,fib}}{P_{u,\exp}}$	$\frac{P_{u,cal}}{P_{u,\exp}}$	Ref.
R2-20-1	20	85×130×2.86	390	228	59.3	825.2	835.56	834.62	1.013	1.011	[16]
R2-100	100	85×130×2.86	390	228	59.3	761.3	793.19	791.44	1.042	1.04	
R2-200	200	85×130×2.86	390	228	59.3	757.5	772.03	769.24	1.019	1.015	
R2-300	300	85×130×2.86	390	228	59.3	793.2	744	740.02	0.938	0.933	
R2-400	400	85×130×2.86	390	228	59.3	725.6	709.15	703.80	0.977	0.97	
R2-500	500	85×130×2.86	390	228	59.3	725.6	665.32	654.96	0.917	0.903	
R2-600	600	85×130×2.86	390	228	59.3	603.4	607.23	595.45	1.006	0.987	
R2-700	700	85×130×2.86	390	228	59.3	537.6	540.88	526.07	1.006	0.979	
R2-800	800	85×130×2.86	390	228	59.3	445.5	463.56	446.79	1.041	1.003	
R2-900	900	85×130×2.86	390	228	59.3	398.5	374.56	357.53	0.940	0.897	
S-20-1	20	120×120×6	360	265	31.5	1115.82	1096.15	1092.46	0.982	0.979	[39]
S-200	200	120×120×6	360	265	31.5	1183.6	1064.22	1051.34	0.899	0.888	
S-300	300	120×120×6	360	265	31.5	1140	1064.96	1032.97	0.934	0.906	
S-400	400	120×120×6	360	265	31.5	1190	1069.85	1010.19	0.899	0.849	
S-500	500	120×120×6	360	265	31.5	1129.9	1041.24	965.87	0.922	0.855	
S-600	600	120×120×6	360	265	31.5	1016.9	990.25	905.97	0.974	0.891	
S-700	700	120×120×6	360	265	31.5	850	922.42	833.14	1.085	0.98	
S-800	800	120×120×6	360	265	31.5	833.33	839.45	747.38	1.007	0.897	
S-900	900	120×120×6	360	265	31.5	723.2	742.34	648.67	1.026	0.897	
Mean									0.961	0.941	
Standard deviation (SD)									0.052	0.055	
Coefficient of variation (COV)									0.053	0.058	